metals

MDPI

Article

Effect of Sulfur on Antimony-Induced High-Temperature Ductility Deterioration of C-Mn Steel

Guilin Sun [1,2], Guochun Dong [1], Sufen Tao [1,2,*], Yunjin Xia [1,2,*] and Chao Chen [2,3]

[1] School of Metallurgical Engineering, Anhui University of Technology, Ma'anshan 243002, China
[2] School of Metallurgical and Ecological Engineering, University of Science and Technology Beijing, Beijing 100083, China
[3] College of Materials Science and Engineering, Taiyuan University of Technology, Taiyuan 030024, China
* Correspondence: ahuttsf@163.com (S.T.); xyjsssss@aliyun.com (Y.X.); Tel.: +86-188-5557-9718 (S.T.); +86-183-5555-3017 (Y.X.)

Abstract: The recycling of steel scrap is becoming more and more developed to save resources and protect the environment. However, impurities such as antimony in steel scrap cannot be economically and effectively removed, resulting in an inevitable accumulation of impurities. Once the impurity concentration exceeds a certain limit, they will have a great impact on the ductility deterioration and hot shortness of steel. It has been shown that sulfide can inhibit the precipitation of residual elements, such as copper at grain boundaries, in steel. The effect of sulfur on the thermoplasticity of antimony-containing C-Mn steel at 700–1100 °C was examined using a Gleeble 1500 thermodynamic simulation device (Gleeble, Poestenkill, NY, USA). Area reduction (RA%) was used to evaluate the thermal ductility. The 0.16 mass % Sb extended the range of the ductile grooves, reducing the RA% at 750–950 °C. Antimony (Sb) was found to segregate at the boundaries tested by an electron probe microanalyzer. Additionally, scanning electron microscopy was used to examine the fracture morphology, which exhibited the characteristics of intergranular failure. In contrast, the addition of sulfur to the steel compensated for the deterioration of the thermal ductility caused by the Sb.

Keywords: antimony and sulfur; hot ductility; grain boundary segregation; tensile test

Citation: Sun, G.; Dong, G.; Tao, S.; Xia, Y.; Chen, C. Effect of Sulfur on Antimony-Induced High-Temperature Ductility Deterioration of C-Mn Steel. *Metals* **2023**, *13*, 130. https://doi.org/10.3390/met13010130

Academic Editor: Carlos Capdevila-Montes

Received: 5 December 2022
Revised: 26 December 2022
Accepted: 5 January 2023
Published: 9 January 2023

1. Introduction

Scrap steel can act as a renewable resource by saving energy and protecting the environment. Compared to traditional iron ore steelmaking, using scrap steel can save a large amount of water, iron ore, coke, and limestone, and it can also significantly reduce the generation of waste water and waste residue [1,2]. As increasing amounts of iron and steel are accumulated, domestic resources and consumption of waste steel are also increasing. An unavoidable problem in improving the efficiency of scrap steel recycling is that the content of residual antimony (Sb) in the steel increases as more scrap steel is recycled, which degrades the performance of the recycled steel [3,4]. The oxygen potential of Sb is lower than that of iron, and therefore cannot be removed via oxidation. At the same time, Sb has a low melting point and is easy to enrich at grain boundaries. In the process of continuous casting and rolling, when the billet is continuously cooled from a high temperature, Sb is isolated on the surface of the billet and the inner grain boundaries, which reduces the cohesion between the surface and the grain boundaries. It is also prone to surface and internal cracks, which affect the quality and yield of continuous casting billets [5–8].

The method currently used to reduce the excessive residual elements in steel in order to control the purity of steel is to use a cold/hot direct reduced iron (DRI), hot pressed iron (HBI), iron carbide, blast furnace hot iron, and other scrap steel substitutes. However, these methods require a large number of high-quality iron resources. As the proportion of recycled scrap steel increases, iron ore resources are becoming increasingly insufficient,

and the index does not address the root cause. Several studies [9–11] have shown that the calcium treatment process can partially remove the residual Sb. However, in the process of steelmaking, calcium reacts preferentially with oxygen and sulfur (S) in the steel, which is prone to substantial carburization, and there are Sb compounds in the slag that require special treatment after the calcium treatment is complete.

Considering that the segregation of Sb at the grain boundaries is the root cause of the deterioration of the steel's properties, the authors of this study focused on inhibiting the segregation of Sb at the grain boundaries. Based on the idea of oxide metallurgy [12–14], Sun [15] found that MnS of appropriate size and shape in the steel can become the heterogeneous nucleation core of the ε-FeSb phase. By controlling the size of the MnS and dispersing them in the steel matrix, the effect of the segregation of Sb at the grain boundaries can be effectively mitigated.

Thus far, there have been only a few reports investigating the effect of sulfur on the mechanical properties of steels that contain Sb. However, based on the facts described above, it is anticipated that MnS may be able to suppress the high-temperature ductility deterioration of low-alloy steel caused by Sb impurities. To clarify this, in this study the combined effect of Sb and S impurities on the high-temperature ductility of C-Mn steel was investigated via a Gleeble thermodynamic simulation machine (Gleeble, Poestenkill, NY, USA). The reduction in area curves, fracture morphologies, microstructures adjacent to the fractures, and the improvement mechanism of increasing the amount of S were analyzed.

2. Materials and Methods

The experimental steel was smelted at 1600 °C by using a ZG-0.025 vacuum induction furnace (Furnace, Xi'an, China) and then cooled to room temperature to obtain the ingot, the chemical composition of which is shown in Table 1. The molten ingot was heated to 1250 °C for 90 min before forging. The forging process was as follows: the initial forging temperature was 1150 °C, the final forging temperature was 800 °C, the hot forging resulted in a round bar with a 15-mm diameter, and the round bar was treated with air cooling after forging. The sample was then heated in a Muffle furnace at 850 °C for 3 h and then cooled in the furnace to remove the forging stress.

Table 1. Chemical composition of experimental steels (wt.%).

No.	C	Si	Mn	P	Als	N	T.O	S	Sb
1	0.17	0.32	1.43	0.008	0.002	0.0010	0.0015	0.008	0
2	0.14	0.27	1.41	0.007	0.004	0.0011	0.0026	0.007	0.13
3	0.13	0.28	1.40	0.008	0.005	0.0008	0.0025	0.027	0.13

After the sample was annealed, it was forged and processed into a bar with a diameter of 12 mm. This bar was further cut and polished in order to accurately process it into a thermal tensile sample with a diameter of 10 mm and length of 120 mm, with threads at both ends. The Gleeble 1500 thermodynamic simulation machine was used to conduct a high-temperature thermoplasticity experiment, and the nitrogen gas was passed into the test module to prevent oxidation. The thermal process is shown in Figure 1. The sample was heated to 1350 °C at a heating rate of 10 °C/s, held for 5 min to achieve uniform temperature, and then cooled to the experimental temperature (700 °C, 750 °C, 800 °C, 850 °C, 900 °C, 1000 °C, and 1100 °C) at a cooling rate of 20 °C/s. Next, the tensile test was carried out at a strain rate of 1×10^{-3} s^{-1}, and argon gas was introduced into the sample chamber a flow rate of 1 L/min. The fracture site was sprayed with water to cool it immediately after the thermal drawing to maintain the fracture morphology and metallographic structure at high temperature.

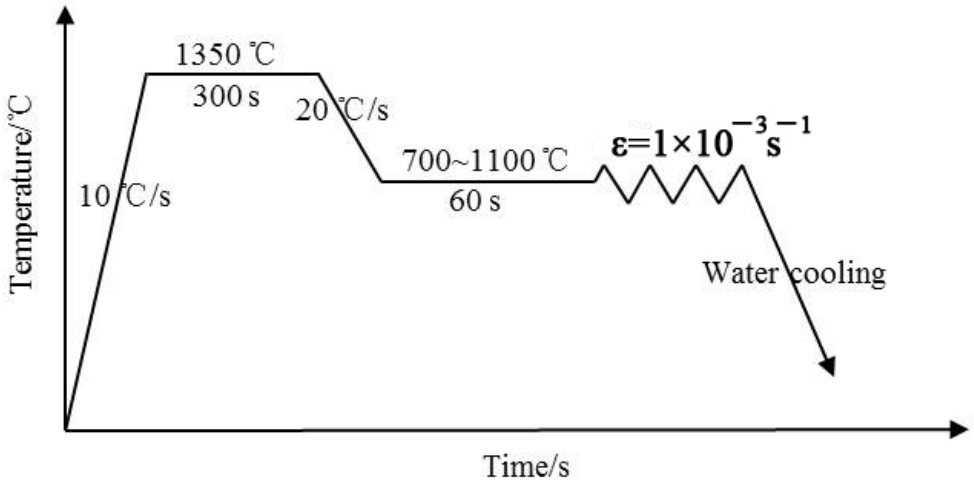

Figure 1. Thermal schedule of the hot tensile test.

In this paper, the thermoplasticity of the steels is mainly measured by the area reduction (RA%). RA can be calculated from Formula (1):

$$RA = [(S0 - Su)/S0] \times 100\% \quad (1)$$

RA—the area reduction, S0—the original cross-sectional area, Su—the minimum cross-sectional area after fracture. The RA corresponding to each experimental temperature was calculated, and the software Origin was used to draw the thermoplastic curves. Scanning electron microscopy was used to photograph the fracture at different temperatures in order to obtain the microscopic morphology of the fracture. Then, metallographic samples were made. The samples were treated with 4% (volume fraction) nitrate alcohol solution and saturated picric acid solution at room temperature. Then, a Leica DMRX optical microscope (Leica, Wetzlar, Germany) was used to observe the fracture tissues. The Sb content at the grain boundaries of the samples that were eroded with the picric acid aqueous solution was quantitatively analyzed using a JXA-8230 electron probe microanalyzer (EPMA, JEOL Ltd., Tokyo, Japan).

3. Results

3.1. Hot Ductility Evaluation

The thermoplastic curve of the steel is shown in Figure 2. In the temperature range of 750–950 °C, the area reduction (RA%) of the C-Mn steel was significantly reduced by the 0.13% Sb content. The addition of S improved the thermal ductility degradation caused by 0.13 mass % Sb. When the S content increased from 0.007 to 0.027 mass %, the RA% of the steel containing 0.13 mass % Sb increased significantly at 750–950 °C. The RA% of steel 1, steel 2, and steel 3 are denoted as RA1, RA2, and RA3, respectively. It was clear that RA1 > RA3 > RA2, and the thermal ductility of steel 2 was primarily due to the addition of Sb, as the content of the other elements in the three steels tested was almost the same. Although the thermal ductility of steel 3 with more S than steel 2 was better than that of steel 2, it was still not as good as that of steel 1 without Sb. This indicates that the addition of S to C-Mn steel containing residual Sb reduces the harmful effect of Sb on the thermal ductility of steel, but it cannot eliminate the harm or even improve the performance. In the continuous casting process, the temperature range with an RA% less than 60% was considered [16,17] as the crack sensitive zone, and the temperature range was considered as having low ductility. Therefore, the low ductility zones of steel 1, 2, and 3 were 731–823 °C, 720–932 °C, and 724–895 °C, respectively. In the area of low thermal ductility, the RA% of each type of steel decreased first and then increased. At 750 °C, the RA% curve of each steel exhibited a trough. The ductility groove of steel 2 containing 0.16% Sb was deeper than that of the other two steels.

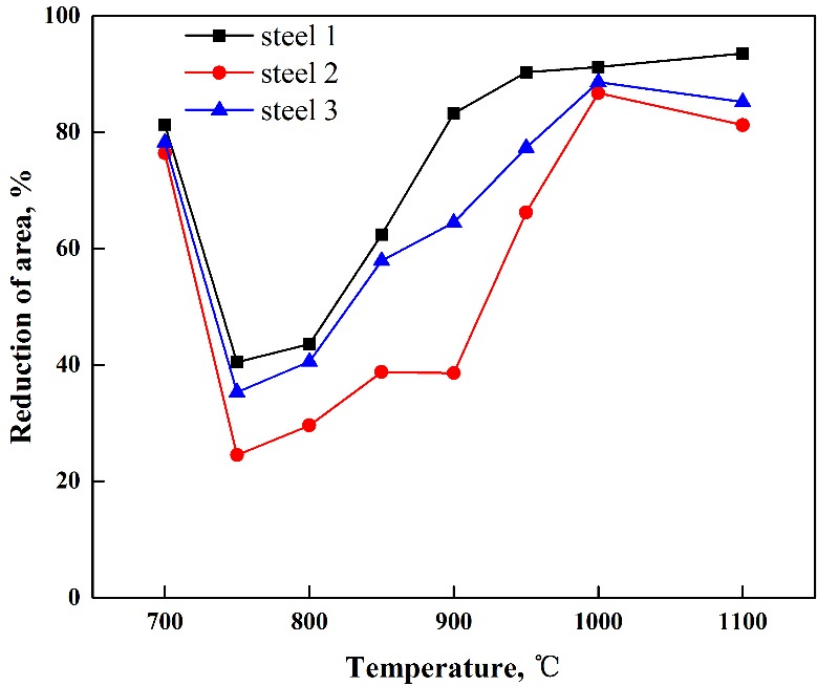

Figure 2. RA values of the steels tensile-tested at different temperatures between 700 and 1100 °C.

3.2. Fracture Morphology

Figure 3 shows the fracture morphologies of all three test steels in the groove. At 750 °C, all the fracture morphologies of each type of steel exhibited the characteristics of intergranular failure, and the size of intergranular block structure represented the austenite grain size. On the surface, steel 2 with 0.13% Sb and an S content of 80 ppm had a more pronounced tendency to intergranular fracture than steel 1 and 3. For example, steel 2 had a smoother fracture surface and a clearer surface. That is, the lower the thermoplasticity of the steel, the greater the tendency toward intergranular fracture.

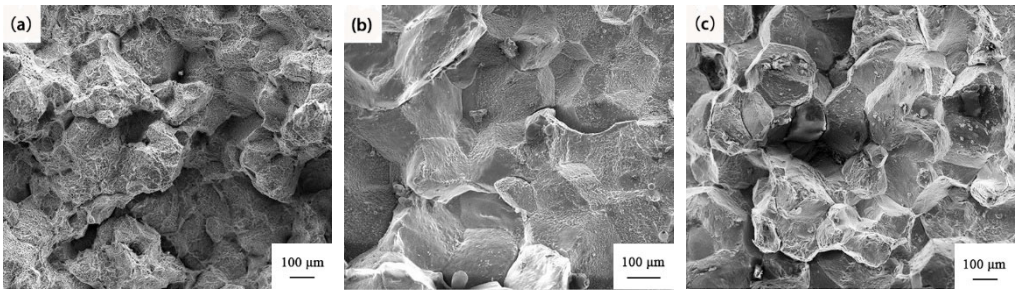

Figure 3. Fracture morphology of different samples tested at 750 °C for (**a**) steel 1; (**b**) steel 2; and (**c**) steel 3.

3.3. Microstructure Observation

Figure 4 shows the microstructure of the longitudinal cross-section near the fracture. At 750 °C, the membranous pre-eutectoid ferrite layer was clearly observed along the austenite grain boundary. The cracks were distributed in the interface between the pro-eutectic ferrite and austenite or inside the pro-eutectic ferrite phase. Because of the difference in deformation between the austenite and pro-eutectic ferrite, the thin and continuous pro-eutectic ferrite along the austenite grain boundary was very unfavorable to the thermoplasticity of steel. Therefore, all the test steels had thermal ductility troughs at 750 °C, and the fracture was consistent with typical intergranular failure, as shown in Figure 3a–c.

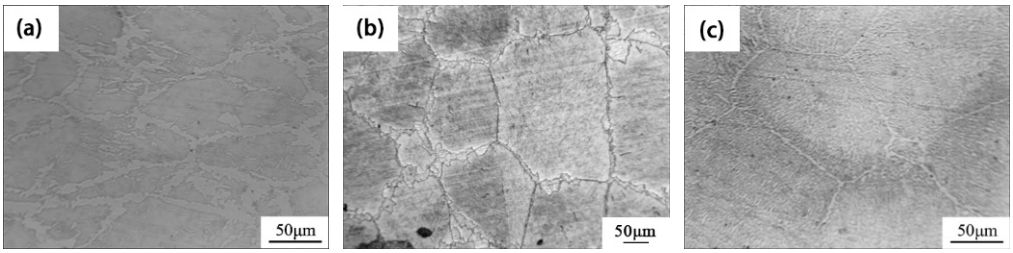

Figure 4. Optical microstructures near the fracture tips of different samples tested at 750 °C for (**a**) steel 1; (**b**) steel 2; and (**c**) steel 3.

3.4. EPMA Analysis

Due to the addition of Sb, the RA% value in steel 1 decreased from 83.2% to 38.6%, particularly at 900 °C. Due to the addition of S, the RA% value in steel 2 increased from 38.6% to 64.5% at 900 °C. Steel 2 was deformed to the point of failure, after which it was quenched with water. One experiment was eroded with picric acid and involved point scanning randomization at grain boundaries using an EPMA, and the other experiment was not picric acid corrosion for random spot scan on the matrix. The results are shown in Table 2 and Figure 5. The Sb was found to have distinct segregation at the grain boundaries. The $(G/M)_{Sb}$ value was 2.0. The grain boundary content/matrix "i" average content was denoted as $(G/M)_i$. The same method was used to treat steel 3, and it was found that the Sb was weakened at the grain boundary and $(G/M)_{Sb}$ was 1.54.

Table 2. Results of quantitative analysis of different samples tested by EPMA (wt.%).

	Point								Average
	1	2	3	4	5	6	7	8	
Grain boundary—steel 2	0.264	0.258	0.272	0.249	0.253	0.262	0.258	0.266	0.2603
Matrix—steel 2	0.137	0.127	0.142	0.132	0.127	0.123	0.139	0.116	0.1304
Grain boundary—steel 3	0.178	0.161	0.183	0.222	0.164	0.224	0.151	0.212	0.1867
Matrix—steel 3	0.129	0.093	0.143	0.132	0.105	0.106	0.139	0.126	0.1216

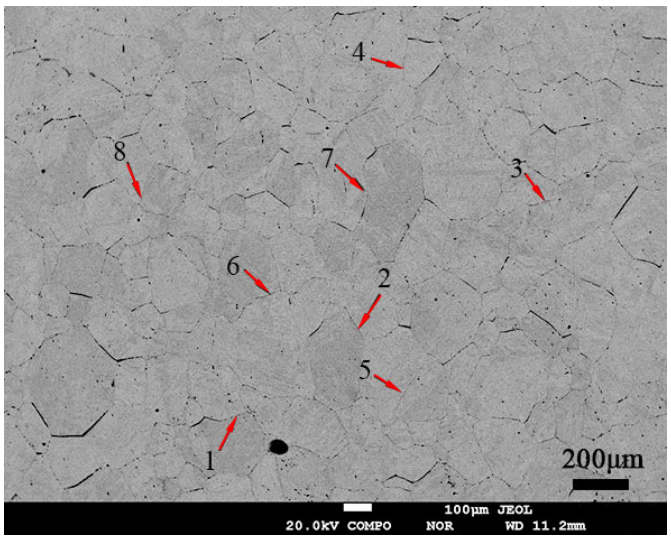

Figure 5. Spot scan by EPMA at grain boundary of steel 2.

4. Discussion

According to the thermoplastic results (the RA value, RA1 > RA2) of steel 1 and steel 2, when Sb was added to the steel, the thermoplasticity of the steel became worse, the hot brittle zone became larger and moved to the high-temperature zone, and the

plastic bottom was deepened. In addition, the EPMA test results showed that there was clear segregation of Sb in steel 2 at the grain boundary, and the average Sb content ratio between the grain boundary and the matrix was $(G/M)_{Sb}$ = 2.0. It has been reported that the segregation behavior of Sb in thermal tensile experiments can be categorized as non-equilibrium segregation, which is a dynamic process that primarily occurs in the cooling process of the solution temperature or after quenching [18]. According to the non-equilibrium segregation theory [19], solute atoms and supersaturated vacancies generated in the tensile process combine to form solute-vacancy complexes, because these complexes have a large segregation capacity. Segregation at grain boundaries is easily achieved, and this degrades the properties of steel. The grain boundary segregation of Sb can reduce the grain boundary energy of steel, weaken the cohesion between grains, accelerate the formation and growth of grain boundary micropores, and hinder the migration of grain boundaries, thus deteriorating the thermoplasticity of steel.

The Force-Stroke rheological curves of steel 1, 2, and 3 samples are shown in Figure 6. The figure indicates that the initial temperature of dynamic recrystallization in steel 1 is 800 °C, the initial temperature of dynamic recrystallization in steel 2 is 850 °C, and that in steel 3 is 800 °C, as shown in Figure 6a–c, respectively. It was clear that the temperature of DRX in steel 2 > steel 1 = steel 3, and the initial temperature of dynamic recrystallization of steel 2 (the highest value) was primarily due to the addition of Sb, as the content of the other elements in the three steels tested was almost the same. This suggests that the addition of Sb can lead to a delay in the dynamic recrystallization of steel. In the dynamic recrystallization process, grain boundary migration occurs, and the movement of grain boundaries can isolate the pores and prevent the consolidation and growth of grain boundary micropores, which is conducive to generating improvements in the thermoplasticity of steel. Therefore, Sb hinders the dynamic recrystallization of steel, thus degrading the thermoplasticity of steel to a certain extent.

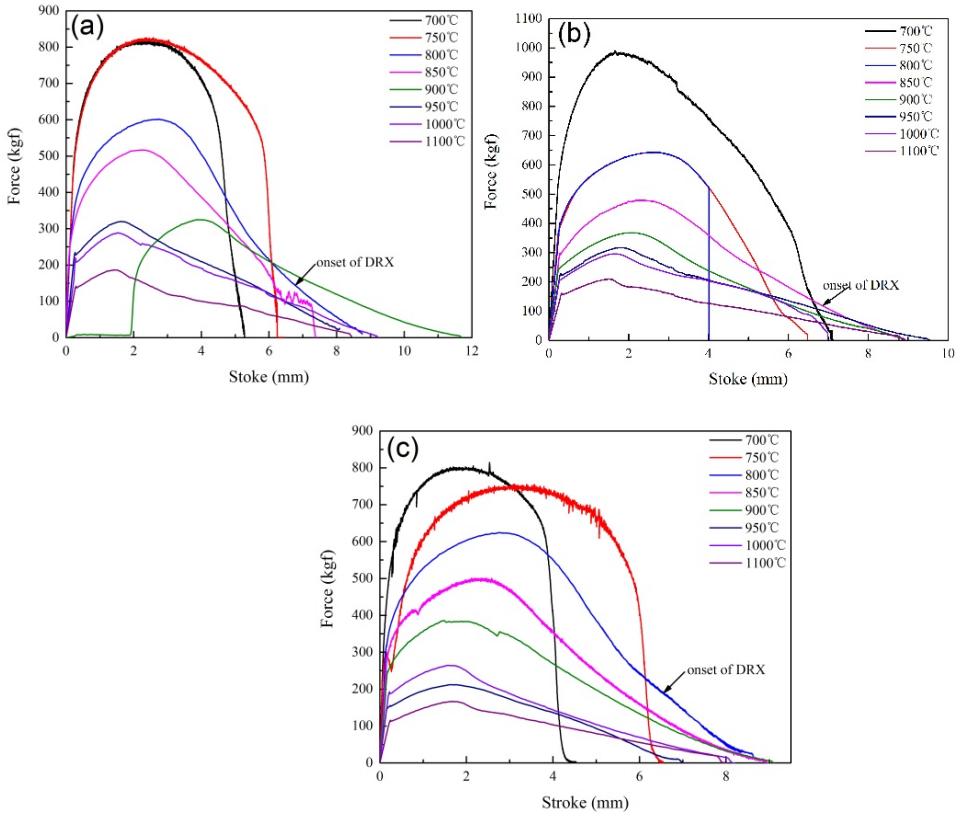

Figure 6. Flow curves of force vs. stroke of different samples tested for (**a**) steel 1; (**b**) steel 2; and (**c**) steel 3.

Suuzuki [20] et al. studied the high-temperature mechanical properties of continuous cast steel. By analyzing the influences of heating temperature, chemical composition, strain rate, holding time, cooling rate, and other factors on strength and plasticity, as well as fracture morphology and the embrittlement mechanism of steel, they divided steel into three brittle temperature zones from the solidification temperature to 600 °C. That is, the first brittle temperature zone ranged from the melting point to 1200 °C, the second brittle temperature zone ranged from 1200 °C to 900 °C, and the third brittle temperature zone ranged from 900 °C to 600 °C. The second brittle temperature region appeared only when the strain rate was greater than 10^{-2} s^{-1}. Under the experimental conditions, the strain rate was low (10^{-3} s^{-1}), and the second brittle temperature zone did not appear. In the third brittle temperature zone, the thermoplastic curves of the experimental steels had similar shapes, and the plastic bottom appeared at 750 °C. With the addition of Sb, the thermoplasticity of C-Mn steel became worse, which not only enlarged the temperature range of the plastic groove, but also made the hot brittle zone shift to a high temperature and deepened the plastic trough. As the Sb content increased, the width and depth of the temperature range of the plastic groove expanded, which indicated that the residual element was an important factor affecting the plastic deterioration in this temperature range.

Liu's [21] study showed that in steel containing Sn (Fe-0.065C-0.0169S-0.68Mn-0.085Cu-0.09Sn), the degree of Sn segregation decreased significantly as the S content increased from 0.0022 wt.% to 0.0169 wt.%, and Sn existed at the interface between the MnS and the matrix. The author's previous experiments [15] revealed that MnS inclusion in steel can be the core of Sb phase precipitation. According to the quantitative detection of Sb at the grain boundary of steel 3 via an electron probe, the addition of S in steel reduced the ratio (G/M) of the average Sb content between the grain boundary and matrix from 2.00 to 1.54. Therefore, when 0.02 wt.% S was added to steel 2, a large number of MnS inclusions formed in the steel. Some of the MnS inclusions with appropriate sizes and shapes became the core of the heterogeneous precipitation of the residual Sb, thus reducing the segregation of Sb at the grain boundary and effectively improving the thermoplasticity of C-Mn containing Sb. Sun [22] et al. verified using a JEM-2100F transmission electron microscope (JEOL Ltd., Tokyo, Japan) that MnS can be the effective heterogeneous nucleation core of the Sb precipitated phase in Sb-bearing steel.

5. Conclusions

The effect of sulfur on antimony-induced high-temperature ductility deterioration of C-Mn Steel was studied. The research results are summarized as follows:

(1) The influence of sulfur on the high-temperature ductility of C-Mn steel was studied using the Gleeble 1500 thermodynamic simulator. Antimony was found to cause the low ductility region to become large, and there was a trough in the RA%-temperature curve at 750 °C.
(2) The addition of S to C-Mn steel containing residual Sb reduced the degradation caused by the Sb to the thermal ductility of the steel, but it did not eliminate the degradation or even improve the performance.

Author Contributions: Conceptualization, G.S. and S.T.; methodology, G.S. and G.D.; formal analysis, S.T., C.C. and Y.X.; investigation, Y.X.; writing—original draft preparation, G.S. and S.T.; writing—review & editing, S.T., C.C. and Y.X. All authors have read and agreed to the published version of the manuscript.

Funding: This research was funded by the National Natural Science Fund [Grant No. 52074001, 52204329], the Anhui Provincial Natural Science Foundation [Grant No. 2108085QE215], and the Natural Science Foundation of Educational Department of Anhui Province [Grant No. KJ2020A0273].

Data Availability Statement: Not applicable.

Conflicts of Interest: The authors declare no conflict of interest.

References

1. Task Group for the Strategic Research on Great Power of Ferrous Metal Mineral Resources. Development situation of ferrous metal resources in China. *Strateg. Stud. CAE* **2019**, *21*, 1–8.
2. Yang, R.W.; Chen, C.; Lin, Y.C.; Zhao, Y.; Zhao, J.; Zhu, J.J.; Yang, S.S. Water model experiment on motion and melting of scarp in gas stirred reactors. *Chin. J. Process Eng.* **2022**, *22*, 954–962.
3. Ramadan, A.; Shash, A.Y.; El-Mahallawi, I.S.; Senk, D.; Mattar, T. Effect of tempcore processing on mitigating problems of tramp elements in low C steel produced from recycled material. *J. Iron Steel Res. Int.* **2015**, *22*, 582–589. [CrossRef]
4. Zhang, L. Influence of residual elements in steel on the quality of CSP products. *Met. Mater. Metall. Eng.* **2009**, *37*, 12–15.
5. Yin, L.; Sridhar, S. Effects of residual elements arsenic, antimony, and tin on surface hot shortness. *Metall. Mater. Trans. B* **2011**, *42*, 1031–1043. [CrossRef]
6. Deng, S. The influence of residual elements to steel quality and its controlling. *Liu Steel Technol.* **2016**, *2*, 10–15.
7. Chen, C.; Cheng, G.G. Delta-ferrite distribution in a continuous casting slab of Fe-Cr-Mn austenitic stainless steel. *Metall. Mater. Trans. B* **2017**, *48*, 2324–2333. [CrossRef]
8. Zhang, X.; Ma, G.J.; Liu, M.K.; Li, Z. Removal of residual element tin in the ferrous metallurgy process: A review. *Metals* **2019**, *9*, 834. [CrossRef]
9. Kitamura, K.; Takenouchi, T.; Iwanami, Y. Removal of impurities from molten steel by CaC_2. *Tetsu-to-Hagane* **1985**, *71*, 220–227. [CrossRef] [PubMed]
10. Tsukihashi, F.; Kuroda, K.; Arakawa, S.; Shoichiro, A.; Nobuo, S. Activity coefficient of antimony and arsenic in molten iron and carbon saturated iron. *Steel Res.* **1994**, *65*, 53–57. [CrossRef]
11. Min, D.J.; Sano, N. Determination of the standard Gibbs energies of formation of Ca_3As_2, Ca_3Sb_2, and Ca_3Bi_2. *Metall. Mater. Trans. B* **1989**, *20*, 863–870. [CrossRef]
12. Takamura, J.; Mizoguhci, S. Roles of oxides in steel performance. In Proceedings of the Sixth International Iron and Steel Congress, Nagoya, Japan, 21–26 October 1990.
13. Mizoguchi, S.; Takamura, J. Control of oxides as inoculants-metallurgy of oxides in steels. In Proceedings of the Sixth International Iron and Steel Congress, Nagoya, Japan, 21–26 October 1990.
14. Yuan, X.B.; Zhong, M.; Wu, Y.W.; Wang, C. Characterizing Inclusions in the Weld Metal of Eh36 Shipbuilding Steel Processed by CaF_2-30 Wt Pct TiO_2 Flux. *Metall. Mater. Trans. B* **2022**, *53*, 656–661. [CrossRef]
15. Sun, G.L. Fundamentals on Precipitation Behavior of Residual Elements Tin and Antimony in Steel. Ph.D. Thesis, University of Science and Technology Beijing, Beijing, China, 2016.
16. Suzuki, H.G.; Nishimura, S.; Imamura, J. Embrittlement of steels occurring in the temperature range from 1000 °C to 600 °C. *Trans. Iron Steel Inst. Jpn.* **1984**, *24*, 169–177. [CrossRef]
17. Suzuki, H.G.; Nishimura, S.; Imamura, J.; Nakamura, Y. Hot ductility in steels in the temperature range between 900 and 600 °C. *Tetsu-to-Hagane* **1981**, *67*, 1180–1189. [CrossRef] [PubMed]
18. Yuan, Z.X.; Guo, A.M.; Liu, J.; Shen, D.D.; Jia, J.; Song, S.H. Antimony grain boundary segregation and its suppression by cerium in Fe-2%Mn-Sb structural steels. *Acta Metall. Sin.* **2003**, *16*, 175–182.
19. Faulkner, R.G. Non-equilibrium grain-boundary segregation in austenitic alloys. *J. Mater. Sci.* **1981**, *16*, 373–383. [CrossRef]
20. Suzuki, H.G.; Nishimura, S.; Nakamura, Y. Improvement of hot ductility of continuously cast carbon steels. *Trans. Iron Steel Inst. Jpn.* **1984**, *24*, 54–59. [CrossRef]
21. Liu, Z.Z.; Kuwabara, M.; Satake, R. Effect of Sn on microstructure and sulfide precipitation in ultra low carbon steel. *ISIJ Int.* **2009**, *49*, 1087–1093. [CrossRef]
22. Sun, G.L.; Fan, D.D.; Tao, S.F. Identification of antimony precipitates in Sb-bearing C-Mn steel. *Metall. Mater. Trans. B* **2021**, *52*, 576–579. [CrossRef]